Science Press

ARTICLE

Deuterium Retention Behavior in W-Fe-Ni Alloy

Ji Fuhao[1,2],   Jiang Yingwu[1,3],   Chang Yu[2],   Yan Jun[1],   Jiang Chunli[1],   Wu Jiliang[1],   Li Qiang[1],   Zhang Xiangdong[2],   Ye Xiaoqiu[1]

[1] Science and Technology on Surface Physics and Chemistry Laboratory, Mianyang 621907, China; [2] Institute of Materials, China Academy of Engineering Physics, Mianyang 621908, China; [3] Institut Franco-Chinois de L'Energie Nucléaire, Sun Yat-Sen University, Zhuhai 519082, China

Abstract: Deuterium retention behavior in W-Fe-Ni alloy was investigated by the gas-phase driven permeation system and thermal desorption tests. The deuterium permeability, diffusion coefficient, solubility, and diffusion activation energy of deuterium in the W-Fe-Ni alloys were investigated. The thermal deuterium charging and thermal deuterium desorption experiments were conducted. Combined with the microstructure characteristics and numerical simulation, the deuterium retention behavior in W-Fe-Ni alloys was studied and the diffusion model of hydrogen isotope in W-Fe-Ni alloy was established to predict the deuterium retention in W-Fe-Ni alloys with different shapes. Compared with the results of thermal desorption tests, the amount of hydrogen isotope retention in W-Fe-Ni alloy can be accurately estimated by the multi-physics field numerical simulation.

Key words: W-Fe-Ni alloy; hydrogen isotope retention; permeation; thermal desorption; numerical simulation

W-Fe-Ni alloy prepared by the liquid-phase sintering in hydrogen atmosphere is a two-phase alloy consisting of tungsten and binder phases (nickel and iron)[1,2]. Due to its high density, high strength, and good ductility, W-Fe-Ni alloy has been widely used in aviation, aerospace, weapons, mechanical engineering, instrument, and electrical industry as the counter-weight, armor piercing, outer rotor, and shielding materials[3-8]. The properties of tungsten alloys are sensitive to the impurity content. Particularly, the hydrogen embrittlement may occur in the sintered alloy with a large amount of hydrogen[9-11], thereby affecting the service properties of the material. The solubility of hydrogen in W is much lower than that in Ni and Fe in W-Fe-Ni alloy, and the hydrogen is mainly enriched in the phase boundary and binder phase. Because the hydrogen content can greatly affect the mechanical properties of the alloy[12-15], the investigation for retention behavior of hydrogen isotopes in W-Fe-Ni alloy is of significance and application potential in evaluating the hydrogen content in the alloy and its influence on the service properties of the alloy.

In this research, the transport of deuterium in W-Fe-Ni alloy was studied by the gas-phase driven permeation. The permeability, diffusion coefficient, and solubility of deuterium in the W-Fe-Ni alloy were obtained, and the hydrogen isotope diffusion model of W-Fe-Ni alloy was also established. The specimen was exposed to D_2 with the pressure of 500 kPa at 773 K for 5 h to obtain the deuterium-saturated W-Fe-Ni alloy. The deuterium retention in W-Fe-Ni alloy was then studied by the thermal desorption spectroscopy. The thermal desorption characteristics of deuterium in the W-Fe-Ni alloy were obtained. The relationship between the deuterium release and desorption temperature was investigated. The retention mechanism of deuterium in W-Fe-Ni alloy was discussed. The experimental deuterium desorption amount was compared with the data obtained from the simulated deuterium charging process to evaluate the accuracy of the diffusion model.

1 Experiment and Numerical Simulation

1.1 Specimen preparation

The W-Fe-Ni alloy with the dimension of Φ12 mm×0.5 mm (Institute of Materials, China Academy of Engineering Physics) was mirror-polished by the 400#~2000# silicon carbide abrasive paper. The thickness of specimen after

polishing was 0.456 and 0.442 mm. Then, the polished W-Fe-Ni alloy was ultrasonically rinsed in distilled water and dried by the argon gas for the gas permeation tests and thermal desorption tests. The specimens were placed in a quartz tube preheated to 1273 K at heating rate of 10 K/min with the vacuum degree >5.0×10^{-5} Pa, kept for 1 h, and then cooled to room temperature. Subsequently, the scanning electron microscope (SEM) was used for microstructure observation.

1.2 Permeation experiment

The permeation experiments were conducted by the gas-phase driven permeation system, as shown in Fig. 1. The upstream vacuum coupling radius (VCR) seal equipment containing the mechanical pump, pressure gauge, and LaNi$_5$ deuterium storage bed was used. In the downstream system equipment, a molecular pump set and a quadrupole mass spectrometer (QMS) were used to measure the signal of the gas ion flow through the specimen. The resistance heating furnace was used to heat the penetration tool. The K-type thermocouple was closely attached to VCR to monitor the temperature.

The experiment process was as follows. (1) Air tightness test. After the installation was completed, the helium gas with the pressure>101.3 kPa was measured in the upstream VCR equipment. The helium gas was measured in the downstream vessel by QMS. If the helium ion signal is at the same level as that of the helium background, the VCR equipment has a good sealing performance. (2) Degassing. The heating furnace was used to heat the VCR equipment to the initial temperature (873 K) of the penetration experiment, and the heating belt was used to heat the downstream pipeline to reduce H$_2$ and H$_2$O as much as possible. The downstream vacuum was reduced to 1×10^{-6} Pa. (3) Penetration test. The deuterium gas of 100 kPa was charged into the upstream equipment, and the time of deuterium gas charging was recorded. The mass spectrometer signals were observed during the experiment. When the deuterium gas signal was stable, the upstream deuterium gas was removed, and the continuous vacuum was conducted to reduce D$_2$ and HD of the system, i. e., the permeation test at the specific temperature was completed. After the specimen was heated to other designed temperatures, the abovementioned processes were conducted again. (4) Collection of the mass spectrometer signal data at

different temperatures. After the data processing, the permeation parameters of deuterium in the W-Fe-Ni alloy were obtained.

1.3 Deuterium charging and deuterium thermal desorption experiment

The deuterium charging experiment was conducted in the high-pressure gas-solid reaction experiment system (Science and Technology on Surface Physics and Chemistry Laboratory), and the schematic diagram of the system is shown in Fig. 2. The system is mainly composed of the precision pressure gauge, vacuum gauge, ZrCo deuterium storage bed, reactor, and vacuum pump.

The process of hot charging experiment was as follows. (1) Air tightness test. Firstly, the annealed tungsten alloy was placed in the stainless steel reactor, and the corresponding valve was closed. Then the vacuum was pumped to <5 Pa, and the air tightness of the system was tested. (2) Pipeline gas cleaning. D$_2$ was stored in the ZrCo storage bed, heated, and then entered into the standard vessel. The pipe system was cleaned three times by D$_2$ of 1×10^4 Pa before each experiment. (3) Thermally charged deuterium experiment. After cleaning, the deuterium gas was pumped out and heated to 773 K at heating rate of 10 K/min. The specimens were exposed to D$_2$ with the pressure of 5×10^5 Pa at 773 K for 5 h to obtain the deuterium-saturated W-Fe-Ni alloy. After the heat preservation was completed, the reactor was cooled to room temperature.

After the deuterium charging experiment was completed, the specimen was placed for 5 d, and then the gas-phase thermal desorption tests were conducted. The system was equipped with a QMS to detect and quantitatively analyze the released gas components after the specimen was heated. The specimen was placed in a vacuum quartz tube with the vacuum pressure of more than 1×10^{-5} Pa at room temperature, and then heated to 1273 K at the heating rate of 10 K/min. The deuterium gas released from the specimen was monitored in real time by QMS.

1.4 Data processing

The data processing was conducted according to Eq.(1), as follows:

$$J=-D(\nabla C) \qquad (1)$$

where C is the concentration of solid solution hydrogen, J is the diffusion flux (the number of substances diffused through the section of unit area per unit time), and D is the diffusion coefficient. Combined with Sievert's law, the steady-state permeation flux of hydrogen in the material can be obtained, as follows:

$$J = \frac{DS}{d}\left(\sqrt{p_h} - \sqrt{p_l}\right) \qquad (2)$$

where S is the solubility of hydrogen in the material; d is the thickness of the material; $\sqrt{p_h}$ and $\sqrt{p_l}$ are the pressures of hydrogen at the upstream and downstream ends of the system equipment, respectively. Under the experimental conditions of $p_h \gg p_l$, the permeability (ϕ) formula of hydrogen in the material is $\phi = DS$, and it can be transformed into Eq.(3), as

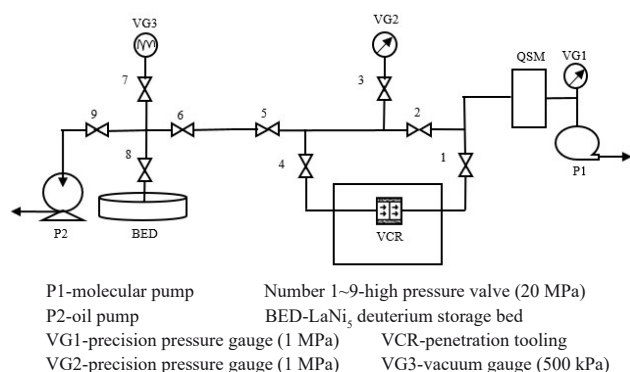| P1-molecular pump | Number 1~9-high pressure valve (20 MPa) |
P2-oil pump	BED-LaNi$_5$ deuterium storage bed
VG1-precision pressure gauge (1 MPa)	VCR-penetration tooling
VG2-precision pressure gauge (1 MPa)	VG3-vacuum gauge (500 kPa)

Fig.1 Schematic diagram of gas-phase permeation system

1#~10#-high pressure valve (20 MPa)   D-thin film capacitance gauge (1333 Pa)
A-mechanical dry pump   E-metal reactor
B-precision pressure gauge (0.1 MPa)   F-precision pressure gauge (6 MPa)
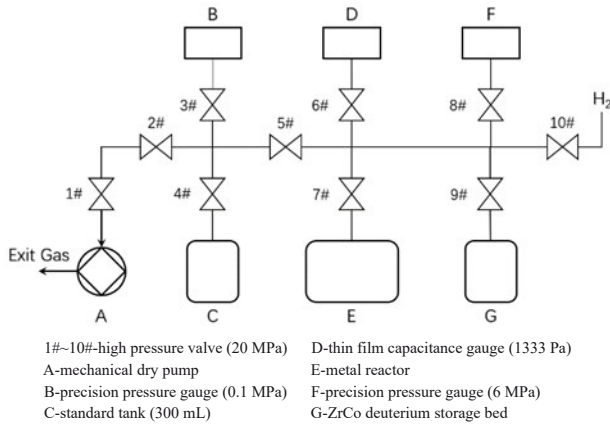C-standard tank (300 mL)   G-ZrCo deuterium storage bed

Fig.2 Schematic diagram of high-pressure gas-solid reaction experimental system

follows:

$$J = \frac{\phi}{d}\sqrt{p_h} \qquad (3)$$

Before the permeation experiment, the ion signal strength of QMS was calibrated by the standard deuterium leak and the relationship between the deuterium ion intensity (I) and leakage rate (L) can be obtained, as follows:

$$L = 4.56 \times 10^3 I \qquad (4)$$

According to the definition of leakage rate, L can be expressed as the variation of pressure in unit time (dt) in the chamber with a certain volume (V):

$$L = V\frac{dp}{dt} = RT\frac{dn}{dt} \qquad (5)$$

where p is the pressure; n is the reaction order; R is the ideal gas constant; T is the permeability temperature. Combined with the definition of permeability flux $J = 1/A \cdot dn/dt$, Eq.(6) can be obtained[16], as follows:

$$J = \frac{L}{RTA} \qquad (6)$$

where A is the permeability area of the specimen. Therefore, the calculation formula of permeability can be obtained, as follows:

$$\phi = \frac{Ld}{RTA\sqrt{p}} = \frac{4.56 \times 10^3 Id}{RTA\sqrt{p}} \qquad (7)$$

The diffusion coefficient of deuterium (D) in the material can be determined by the time-lag method[17], as follows:

$$D \approx \frac{d^2}{6\tau} \qquad (8)$$

where τ corresponds to the time when 63% of the steady-state permeability flux is reached according to the permeability flux curve[18].

The solubility S, diffusion coefficient D, and permeability ϕ of hydrogen isotopes in the structural materials in a certain temperature range can be transformed into the Arrhenius formula type, as follows:

$$K(T) = A_0 \exp\left(-\frac{E}{RT}\right) \qquad (9)$$

$$S(T) = \frac{\phi(T)}{D(T)} = \frac{\phi_0}{D_0}\exp\left(\frac{E_D - E_\phi}{RT}\right) \qquad (10)$$

where K represents S, D, and ϕ indicators; A_0 is the pre-exponential factor of S, D, and ϕ indicators, and it can be divided into S_0, D_0, and ϕ_0, respectively; E is activation energy of S, D, and ϕ indicators, and it can be divided into E_S, E_D, and E_ϕ, respectively.

1.5 Numerical simulation method

The permeability, diffusion coefficient, and solubility of deuterium in the W-Fe-Ni alloy were obtained through the penetration experiments. In order to measure the retention of hydrogen isotopes in the specimens, the diffusion model of hydrogen isotopes in tungsten-based alloy was established by the parameters obtained from the permeation experiment, and the desorption parameters were obtained from the deuterium-thermal desorption experiment with thermal filling to verify the rationality of the model. This numerical simulation model provides technical support to evaluate the hydrogen isotope retention in W-Fe-Ni alloy under different working conditions.

The W-Fe-Ni disc specimen with the dimension of $\Phi12$ mm×0.5 mm possesses the axisymmetric properties. During the process of thermal charging and standing, the hydrogen isotope gas was adsorbed on the surface and desorbed from the surface, respectively. Without the consideration of the effect of material defects, the hydrogen isotope transport process in the specimen is mainly dominated by the diffusion. Therefore, the model can be established, as follows:

$$\frac{\partial C}{\partial t} + \nabla \cdot (D_T \nabla C) = 0 \qquad (11)$$

where C is the concentration of hydrogen isotope atoms in the specimen, and D_T is the atomic diffusion coefficient in the material.

The process of hydrogen isotope gas dissociation and atomic recombination mainly occurs on the material surface, which can be expressed by Sievert's law. In the process of thermal charging, the process of molecular dissociation and atomic recombination is considered to be in the dynamic equilibrium. Thus, Eq.(12) can be obtained, as follows:

$$C = S\sqrt{P} \qquad (12)$$

where S is the atomic solubility in the material and P is the thermal charging pressure. During the experiment, the pressure fluctuation in the reactor was ignored due to the weak hydrogen absorption capacity of the specimen and the basically unchanged thermal charging pressure.

The partial pressure of hydrogen in the atmosphere is low during the specimen standing process, resulting in the neglection of the recombination on surface. Table 1 shows the related parameters for numerical simulation.

2 Results and Discussion

2.1 Micromorphology

Fig.3 and Fig.4 show X-ray diffraction (XRD) patterns of W-Fe-Ni alloys before and after annealing, respectively. It can be seen that the annealing does not influence the characteristic peak of W. The (110), (200), (211), and (220) diffraction peaks of pure tungsten can be observed at $2\theta=40°$, 58°, 73°, and 87°, respectively. No other phases can be detected, which

Table 1 Related parameters in numerical simulation

Parameter	Value	Ref
Diameter, Φ/mm	12	-
Thickness, d/mm	0.5	-
Room temperature, T_1/K	293	-
Experiment temperature, T_2/K	773	-
Diffusion, D/m^2·s^{-1}	$3.7\times10^{-8}\exp\left(\dfrac{-0.333}{kT}\right)$	-
Solubility, S/mol·m^{-3}·Pa$^{-0.5}$	$2.0\times10^{-1}\exp\left(\dfrac{-0.268}{kT}\right)$	-
Recombination coefficient, R/m^4·s^{-1}	$3.2\times10^{-15}\exp\left(\dfrac{-1.16}{kT}\right)$	[19]

Note: k is the Boltzmann constant.
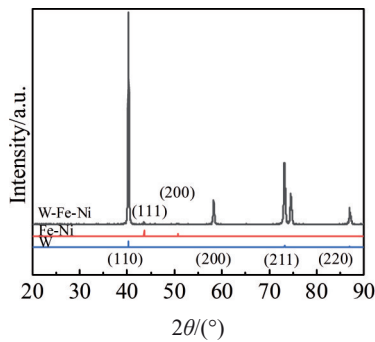
Fig.3 XRD patterns of W-Fe-Ni alloy before annealing and referenced alloys
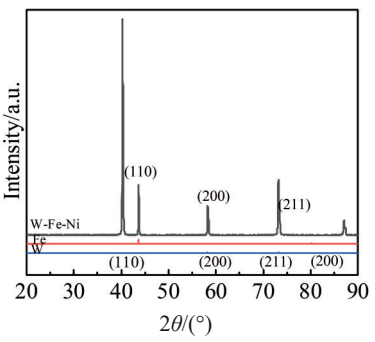

Fig.4 XRD patterns of W-Fe-Ni alloy after annealing and referenced alloys

indicates the complete insolubility of W and binder phase.

Fig.5 and Fig.6 show SEM morphologies of W-Fe-Ni alloys before and after annealing, respectively. There is an obvious interface between the binder phase (Fe-Ni) and the tungsten metal particles in the original W-Fe-Ni alloy, because it is difficult for the binder phase (Fe-Ni) to diffuse into tungsten during sintering due to the body-centered cubic structure and high melting point of tungsten.

As shown in Fig. 5 and Fig. 6, the boundary between the binder phase and tungsten particles in the alloy changes significantly after annealing at 1273 K, and the needle-like structure of W phase grows towards the binder phase. Fig. 7 shows the backscattered SEM morphology and element distributions of W-Fe-Ni alloy after annealing. Generally, the recrystallization temperature of tungsten is about 1573 K, and

the annealing at 1273 K does not have a significant effect on the microstructure. Lei et al[20] observed the specific phenomenon, which is similar to the results in this research, and believed that the carbon impurity in W-Fe-Ni alloy is the necessary condition for the occurrence of this phenomenon.

The element content in different regions of the alloy was determined by the energy dispersive spectroscopy (EDS), as shown in Fig.8. In Fig.8a, point 2 is located at the W particle, point 1 is located located at the protruding area in the extension region of the W particle, point 6 is located in the extension region, and point 3 is located at the interface region between the binder phase and W particles. By comparing EDS spectra of point 2 and point 6, it can be seen that the composition of the two points is mainly W, and the carbon content in the extended region (point 6) is slightly higher. The
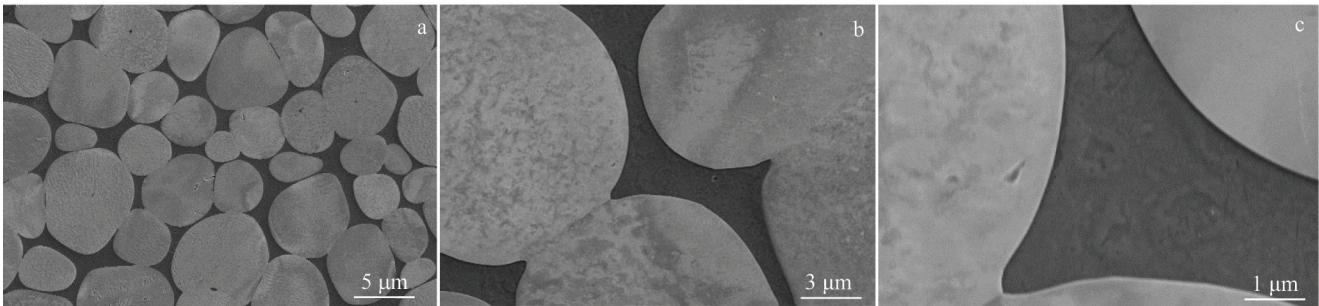

Fig.5 SEM morphologies of W-Fe-Ni alloy before annealing
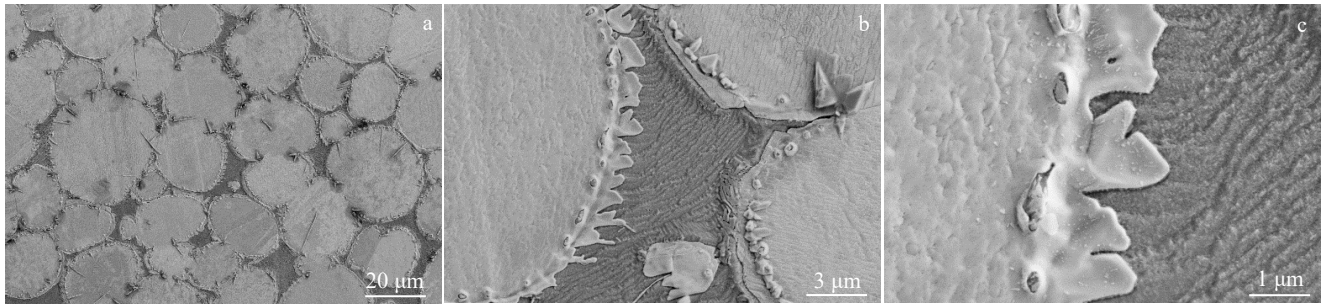
Fig.6   SEM morphologies of W-Fe-Ni alloy after annealing at 1273 K
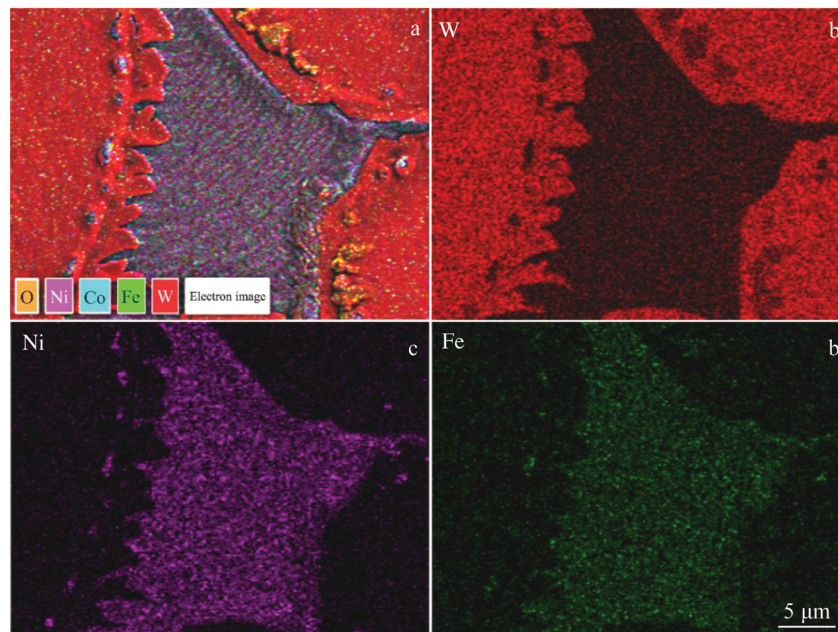

Fig.7   SEM backscattered electron morphology (a) and element distributions of W (b), Ni (c), and Fe (d) in W-Fe-Ni alloy after annealing at 1273 K

boundary between the binder phase and W particles (point 3) is rich in Ni, and it also contains the W, Fe, O, and C elements of high content. This result indicates that the binder phase is the main component in this Fe/Ni-rich region. However, due to the high temperature heating, some tungsten atoms in the metal particles are also integrated into the binder phase, forming the W-Fe-Ni-O multi-binder alloy. The oxygen impurity only exists in the binder phase, and it is the main component of the binder impurity. It can be seen from Fig. 8e that there are W, Fe, and Ni elements at the bulge point in the extension region of W particles, the proportion is relatively uniform, and the impurities barely exist. This may be due to the outward growth of tungsten metal particles during the annealing, and the binder phase at the original boundary is wrapped by the extended tungsten metal particles. In conclusion, there is a certain proportion of carbon in the tungsten particles (point 2), binder phase (point 3), and extended needle-like structure (point 6), indicating that the presence of carbon has an important effect on the microstructure changes of W alloy after annealing. Lei et al[20]

believed that the acicular phase (corresponding to the point 6) and the shell lamellar phase around the tungsten particles (corresponding to point 3) are the same substance of A_6B_6C type carbides, and their chemical composition can be approximately considered as $(Ni, Fe)_6W_6C$. The acicular precipitation normally grows on the shell, and the precipitated acicular phase in this research is mainly composed of W after annealing at 1273 K with furnace cooling. The shell-like phase around the W particles (point 3) can also be approximately considered as the A_6B_6C type carbide, but it is rich in oxygen.

2.2 Deuterium permeation

The deuterium ion current signals detected by QMS in the deuterium permeation process of tungsten alloys at different temperatures (673~873 K) are shown in Fig. 9. The peak ion current shows a decreasing trend, and at each temperature point of penetration, the ion current is at the balance state.

The penetration parameters of permeability (ϕ), diffusion coefficient (D), and solubility (S) of W-Fe-Ni alloys are shown in Fig. 10, Fig. 11, and Fig. 12, and they are obtained
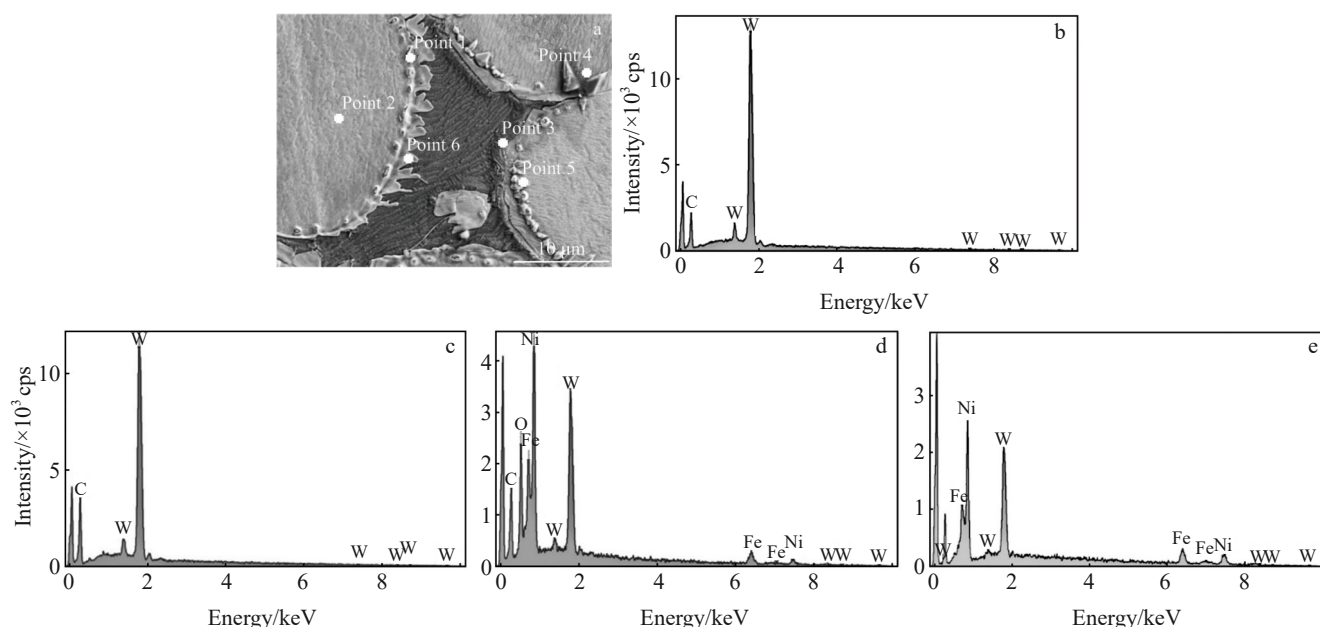
Fig.8   SEM morphology (a) and EDS spectra of points marked in Fig.8a (b~e) of W-Fe-Ni alloy after annealing at 1273 K: (b) point 2; (c) point 6; (d) point 3; (e) point 1
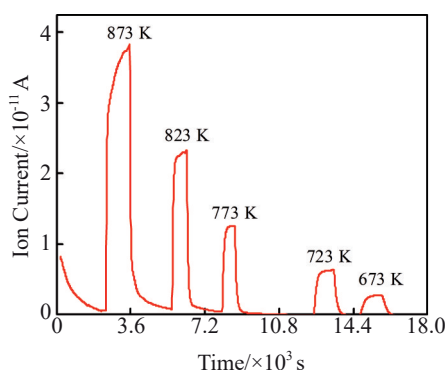

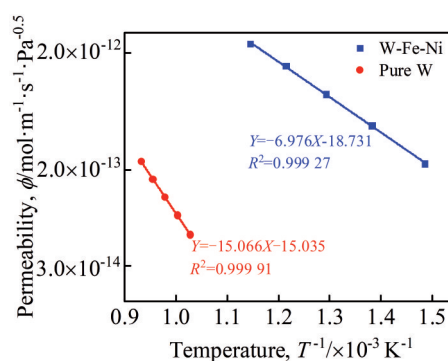Fig.9   Reltionship between ion flow intensity and time

Fig.10   Relationship between deuterium permeability ϕ and temperature T

based on Eq.(13~15), respectively:

$$\phi = 7.3 \times 10^{-9} \exp\left(-\frac{0.601}{kT}\right) \tag{13}$$

$$D = 3.7 \times 10^{-8} \exp\left(-\frac{0.333}{kT}\right) \tag{14}$$

$$S = 2.0 \times 10^{-1} \exp\left(-\frac{0.268}{kT}\right) \tag{15}$$

For comparison, the penetration parameters of permeability (ϕ), diffusion coefficient (D), and solubility (S) of pure tungsten are also shown in Fig. 10, Fig. 11, and Fig. 12, and they are obtained based on Eq.(16~18), respectively:

$$\phi = 2.0 \times 10^{-7} \exp\left(-\frac{1.29}{kT}\right) \tag{16}$$

$$D = 6.8 \times 10^{-5} \exp\left(-\frac{1.16}{kT}\right) \tag{17}$$

$$S = 2.9 \times 10^{-3} \exp\left(-\frac{0.13}{kT}\right) \tag{18}$$

The related data are summarized in Table 1. Fig. 10 shows the relationship between permeability and temperature of

W-Fe-Ni alloy and pure tungsten. The deuterium permeability of W-Fe-Ni alloy is much higher than that of pure tungsten, because the hydrogen isotopes in the binder phase (Fe-Ni) have much higher permeability than those in the tungsten particles[20]. Therefore, the overall permeability of the W-Fe-Ni alloy is higher.

Fig. 11 shows the relationship between the diffusion coefficient and the temperature of W-Fe-Ni alloy and pure tungsten. It can be seen that the deuterium diffusion coefficient of W-Fe-Ni alloy is much larger than that of pure tungsten in the temperature range of 673~873 K. This is obviously related to the high deuterium diffusion coefficient of the bonded phase (Fe-Ni). In addition, the precipitated structure after annealing increases the interfacial area between tungsten particles and the binder phase, which may also promote the interfacial diffusion of deuterium to some extent.

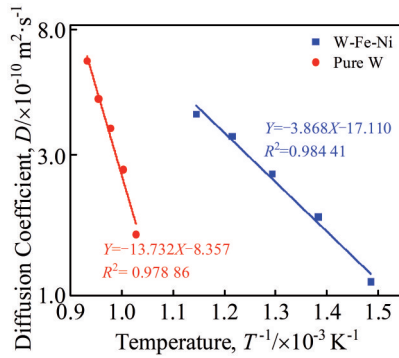Fig. 12 shows the relationship between solubility and

Fig.11 Relationship between deuterium diffusion coefficient D and temperature T
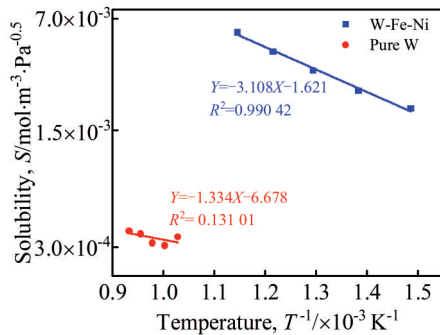

Fig.12 Relationship between deuterium solubility S and temperature T

temperature in W-Fe-Ni alloy and pure tungsten. It can be seen that the deuterium solubility of W-Fe-Ni alloy is much higher than that of the pure tungsten, suggesting that the deuterium solubility in the binder phase (Fe-Ni) is much higher than that of in pure tungsten. Thus, the dissolution process of deuterium in the alloy is mainly dominated by the alloy composition of the binder phase.

2.3 Numerical simulation and thermally charged deuterium experiment

The variation of deuterium in W-Fe-Ni alloy was simulated by the finite element method (FEM) with thermal charging at 773 K and 500 kPa for 5 h and releasing at room temperature
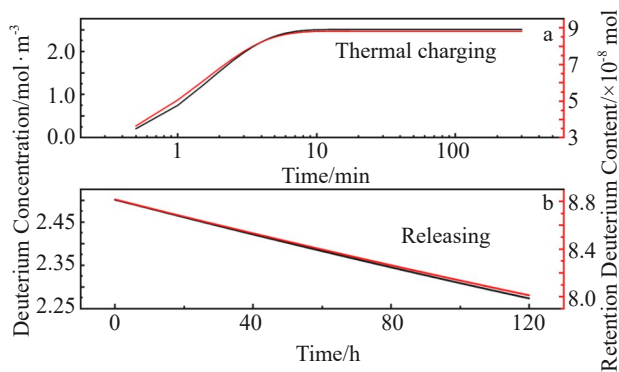

Fig.13 Variation of deuterium concentration and retention deuterium content of W-Fe-Ni alloys during thermal charging process (a) and releasing process (b)
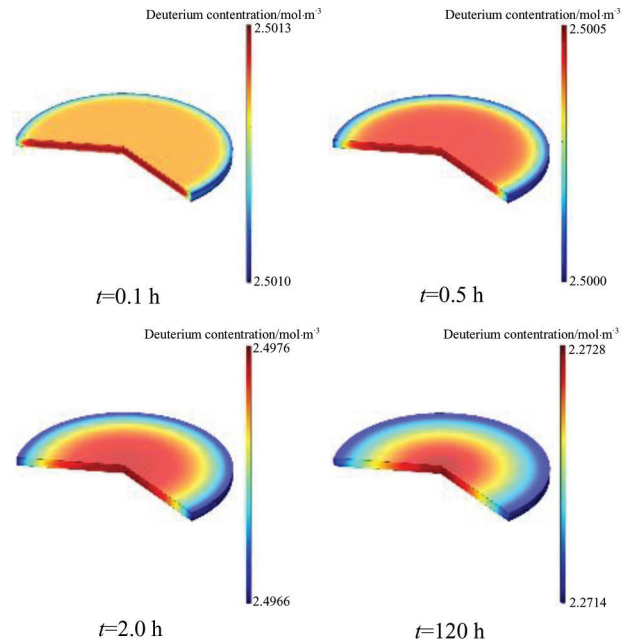

Fig.14 Deuterium concentration distribution during releasing process

for 5 d, as shown in Fig. 13 and Fig. 14. It is found that the deuterium in W-Fe-Ni alloy reaches the saturation after 10 min, the deuterium retention is 8.817×10^{-8} mol, and the average deuterium concentration is 2.50 mol/m^3. The large specific surface area and ultra-thin thickness result in the rapid absorption phenomenon of W-Fe-Ni alloy. Then the average deuterium concentration decreases to 2.274 mol/m^3 after standing for 5 d. The residual deuterium retention decreases to 8.012×10^{-8} mol, and the deuterium loss ratio is 9.13%. This result can be explained by the following reasons. (1) The binder phase (Fe-Ni) of W-Fe-Ni alloy plays a leading role in the dissolution and diffusion of deuterium. In the hot charging process, the deuterium quickly reaches the saturation in W-Fe-Ni alloy, and it is also released quickly at room temperature. (2) The deuterium is enriched on the tungsten particles and the interface between tungsten particles and the binder phase. After the high-temperature annealing, the total area of the interface between the tungsten particles and the binder phase is increased, and the deuterium is released along the interface between the binder phase and the W particles. These two reasons cause the rapid saturation of thermally charged deuterium in the W-Fe-Ni alloy, and partial weakly bonded deuterium is released during the standing process at room temperature.

2.4 Deuterium thermal desorption

The deuterium thermal desorption tests were conducted on the deuterium specimens after the thermally charged deuterium experiment and standing for 5 d. A high desorption peak appears at 620.15 K, and the peak shape is consistent with the Gauss distribution, as shown in Fig. 15. This result indicates that the deuterium in W-Fe-Ni alloy can be removed by annealing treatment below 873 K.
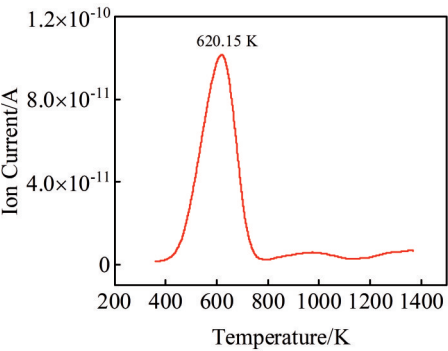
Fig.15　Relationship between ion current and temperature during thermal desorption

Table 2　Experiment and simulated results of deuterium release amount (×10⁻⁸ mol)

Experiment	Simulation
1.572	8.009

The thermal desorption energy of deuterium can be obtained by Eq.(19)[21], as follows:

$$\ln r = (\ln v_n + n \ln \theta) - \frac{E_d}{RT} \tag{19}$$

where r is the thermal desorption rate, v is the desorption rate constant, n is the reaction order, θ is the coverage degree, and E_d is the thermal desorption activation energy. The thermal desorption activation energy E_d of deuterium in W-Fe-Ni specimen is calculated to be 0.35 eV.

In order to verify the accuracy of the model based on FEM, the actual deuterium desorption amount measured in the thermal desorption experiment was compared with the simulated results. Firstly, the signal intensity of deuterium particle flow under different pressures was measured by the standard leak holes, and the relationship between ion current and the deuterium leakage rate Q is obtained by Eq.(20), as follows:

$$Q=0.547I-0.06 \tag{20}$$

The deuterium amount can be deduced from the measured deuterium ion current and the conversion relationship between signal intensity and leakage rate.

The calculation results are shown in Table 2. It can be seen that the experiment and simulation results are in the same order of magnitude, and the simulation result is larger than the experiment one. The error may come from the ideal assumptions of FEM simulation. Firstly, the thermal absorption pressure slightly decreases during the hot filling experiment, but it is considered as a constant in the simulation. Secondly, the material defect can influence the transport of hydrogen isotope in W-Fe-Ni alloy, but the influence is ignored in the simulation. Considering these factors and based on the experiment results of permeability parameters, the retention amount of hydrogen isotopes in W-Fe-Ni alloy can be quickly estimated.

3　Conclusions

1) W-Fe-Ni alloy prepared by the liquid-phase sintering in

hydrogen atmosphere is a two-phase alloy consisting of W and binder phase (Fe-Ni). During the annealing at 1273 K and cooling in furnace, W extends to the binder phase and a needle-like phase, which mainly consists of W, is precipitated. The layered phase consisting of binder phase, W, C, and O appears around the W particles. The presence of carbon impurity has an important effect on the formation of these phases.

2) The solubility constant, diffusion activation energy, and activation energy for the permeation of deuterium in W-Fe-Ni alloy are lower than those of pure tungsten, because the Fe-Ni alloy in the binder phase has a higher deuterium permeability, which plays a leading role in the deuterium permeation process of the alloy.

3) The saturated retention of deuterium in W-Fe-Ni alloy is about 2.50 mol/m³, and the deuterium loss ratio is 9.13% after standing process at room temperature for 5 d. The deuterium thermal desorption peak of the W-Fe-Ni alloy is around 620.15 K, and the activation energy of deuterium thermal desorption is 0.35 eV. The deuterium in W-Fe-Ni alloy can be effectively removed by annealing below 873 K for the alloys with thickness of 0.5 mm.

References

1　Şahin Y. *Journal of Powder Technology*[J], 2014, 2014: 764 306
2　German R M, Suri P, Park S J. *Journal of Materials Science*[J], 2009, 44(1): 1
3　Pang Qianlie. *China Tungsten Industry*[J], 2000, 15(4): 34 (in Chinese)
4　Fan Jinglian, Huang Baiyun, Wang Denglong *et al. Rare Metal Materials and Engineering*[J], 2001, 30(6): 401 (in Chinese)
5　Donten M, Cesiulis H, Stojek Z. *Electrochimica Acta*[J], 2000, 45(20): 3389
6　German R M, Bose A. *120th Annu Meet Miner Met Mater Soc* [C]. New Orleans: TMS, 1991: 53
7　Jiao Z H, Kang R K, Dong Z G *et al. International Journal of Refractory Metals and Hard Materials*[J], 2019, 80: 114
8　Deng S H, Yuan T C, Li R D *et al. Powder Technology*[J], 2017, 310: 264
9　Wang Peng, Liu Kai. *Heat Treatment of Metals*[J], 2015, 40(5): 10 (in Chinese)
10　Gumbsch P. *Journal of Nuclear Materials*[J], 2003, 323(2-3): 304
11　Symons D M. *Metallurgical and Materials Transactions A*[J], 1997, 28(3): 655
12　Powell G L. *Analytical Chemistry*[J], 1972, 44(14): 2357
13　Zhou Guoan, Lin Guobiao, Lai Heyi *et al. Heat Treatment of Metals*[J], 1995, 20(5): 13 (in Chinese)
14　Zhu Guiseng, Liu Mingcheng, Lin Zhongjie *et al. Metallurgica Sinca*[J], 1981, 17(1): 39 (in Chinese)
15　Wu Aihua. *Thesis for Master*[D]. Changsha: Central South University, 2004 (in Chinese)
16　Wang Bo, Liu Lingbo, Xiang Xin *et al. Journal of Nuclear*

Materials[J], 2016, 470: 30

17　Liu Feng. *Thesis for Doctorate*[D]. Beijing: University of Chinese Academy of Sciences, 2015 (in Chinese)

18　Frauenfelder R. *The Journal of Chemical Physics*[J], 1968, 48(9): 3955

19　Hu A, Hassanein A. *Journal of Nuclear Materials*[J], 2014, 446(1-3): 56

20　Lei Bingqiang, Zhu Guisen. *Acta Metallurgica Sinca*[J], 1987, 23(3): 182 (in Chinese)

21　Ebihara K I, Kaburaki H. *ISIJ International*[J], 2012, 52(2): 181

W-Fe-Ni合金中的氚滞留行为

纪富豪[1,2]，蒋应伍[1,3]，常　宇[2]，严　俊[1]，蒋春丽[1]，吴吉良[1]，李　强[1]，张向东[2]，叶小球[1]

(1. 表面物理与化学重点实验室，四川 绵阳 621907)

(2. 中国工程物理研究院 材料研究所，四川 绵阳 621908)

(3. 中山大学 中法核工程与技术学院，广东 珠海 519082)

摘　要： 采用气相驱动渗透系统和热脱附试验平台研究了W-Fe-Ni合金中氚的输运行为，获得了氚在合金中的渗透率、扩散系数、溶解度、扩散激活能等参数，进行了合金热充氚及氚热脱附实验，结合微观结构表征及数值模拟，研究了氚在W-Fe-Ni合金中的滞留行为，并建立了氢同位素扩散模型以估算不同形状尺寸的W-Fe-Ni合金中氚滞留量。通过与热脱附实验结果对比，发现使用多物理场数值模拟可以准确地估算W-Fe-Ni合金中氢同位素滞留量。

关键词： W-Fe-Ni合金；氢同位素滞留；渗透；热脱附；数值模拟

作者简介：纪富豪，男，1996年生，硕士生，表面物理与化学重点实验室，四川 绵阳 621907，E-mail：jifuhao19@gscaep.ac.cn